Boise State University
ScholarWorks

Mathematics Faculty Publications and Presentations

Department of Mathematics

10-1-2005

An Iterated Pseudospectral Method for Functional Partial Differential Equations

J. Mead
Boise State University

B. Zubik-Kowal
Boise State University

An Iterated Pseudospectral Method for Functional Partial Differential Equations

J. Mead   B. Zubik–Kowal

December 1, 2003

Abstract. Chebyshev pseudospectral spatial discretization preconditioned by the Kosloff and Tal-Ezer transformation [10] is applied to hyperbolic and parabolic functional equations. A Jacobi waveform relaxation method is then applied to the resulting semi-discrete functional systems, and the result is a simple system of ordinary differential equations $\frac{d}{dt}U^{k+1}(t) = M_\alpha U^{k+1}(t) + f(t, U_t^k)$. Here M_α is a diagonal matrix, k is the index of waveform relaxation iterations, U_t^k is a functional argument computed from the previous iterate and the function f, like the matrix M_α, depends on the process of semi-discretization. This waveform relaxation splitting has the advantage of straight forward, direct application of implicit numerical methods for time integration (which allow use of large time steps than explicit methods). Another advantage of Jacobi waveform relaxation is that the resulting systems of ordinary differential equation can be efficiently integrated in a parallel computing environment. The Kosloff and Tal-Ezer transformation preconditions the matrix M_α, and this speeds up the convergence of waveform relaxation. This transformation is based on a parameter $\alpha \in (0, 1]$, thus we study the relationship between this parameter and the convergence of waveform relaxation with error bounds derived here for the iteration process. We find that convergence of waveform relaxation improves as α increases, with the greatest improvement at $\alpha = 1$ if the spatial derivative of the solution at the boundaries is near zero. These results are confirmed by numerical experiments, and they hold for hyperbolic, parabolic and mixed hyperbolic-parabolic problems with and without delay terms.

Keywords: Hyperbolic, parabolic, functional equations, Chebyshev pseu-

1

dospectral method, Kosloff Tal-Ezer transformation, waveform relaxation, homogeneous Neumann boundary conditions.

1 Introduction

In this paper we study numerical solutions to the linear non-homogeneous initial boundary value problem with functional term

$$
\frac{\partial}{\partial t}u(x,t) = \epsilon\frac{\partial^2}{\partial x^2}u(x,t)+c\frac{\partial}{\partial x}u(x,t)+g(x,t,u_{(x,t)}), \;\; -L{\le}x{\le}L, \;\; 0{<}t{\le}T,
$$
$$
u(x,t) = f_0(x,t), \quad -\tau_0 \le t \le 0, \; -L \le x \le L.
$$

Choices for c and ϵ have vastly different behavior, i.e $\epsilon = 0$ is the hyperbolic one-way wave equation, $c = 0$ is the parabolic heat equation, while both $\epsilon \neq 0$ and $c \neq 0$ is the parabolic advection-diffusion equation. Different types of boundary conditions are required for the two cases $\epsilon \neq 0$ and $\epsilon = 0$. For the parabolic case ($\epsilon \neq 0$) there are two boundary conditions

$$
u(\pm L, T) = f_\pm(t),
$$

while for the hyperbolic case ($\epsilon = 0$) there is one boundary condition

$$
u(L, t) = f_+(t).
$$

Here, $\tau_0 \ge 0$, $L > 0$ and $T > 0$ are given constants, f_0 and $f_\pm$ are given initial and boundary functions while the function $u_{(x,t)}$ for $(x,t) \in [-L,L] \times [0,T]$ is defined by

$$
u_{(x,t)}(\tau) = u(x, t+\tau), \quad \tau \in [-\tau_0, 0], \tag{1.1}
$$

and $g : [-L,L] \times [0,T] \times C([-\tau_0,0], \mathcal{R}) \to \mathcal{R}$ is a continuous function. Equation (1.1) includes, for example, integro-differential equations

$$
\frac{\partial}{\partial t}u(x,t) = \epsilon\frac{\partial^2}{\partial x^2}u(x,t) + c\frac{\partial}{\partial x}u(x,t) + \tilde{g}(x,t,\int_{-\tau_0}^{0} u(x,t+\tau)d\tau), \tag{1.2}
$$

and delay equations

$$
\frac{\partial}{\partial t}u(x,t) = \epsilon\frac{\partial^2}{\partial x^2}u(x,t) + c\frac{\partial}{\partial x}u(x,t) + \tilde{g}(x,t,u(x,t-\tau_0)) \tag{1.3}
$$

2

cp [16, Section 3]. Here, $\widetilde{g} : [-L, L] \times [0, T] \times \mathcal{R} \to \mathcal{R}$ is a continuous function. If $\widetilde{g}$ is given in (1.2) or (1.3) then the function g is

$$g(x, t, v) = \widetilde{g}(x, t, \int_{-\tau_0}^{0} v(s)ds),$$

or

$$g(x, t, v) = \widetilde{g}(x, t, v(t - \tau_0))$$

respectively with $v \in C([-\tau_0 k, 0], \mathcal{R})$. Functional problems like (1.1) are used to model cancer cells in human tumors, see [1]. For other applications in population dynamics we refer the reader to [5].

We study the Chebyshev pseudospectral spatial discretization of (1.1) [7] with the Kosloff and Tal-Ezer transformation [10], together with Jacobi waveform relaxation methods for time integration [2], [3]. The Chebyshev Pseudospectral method is chosen because (1) it has high accuracy, and (2) when used with waveform relaxation, iterations converge more quickly than when finite differences [16]. Waveform relaxation methods are chosen because (1) they are efficient in parallel computing environments, and (2) they allow direct application of implicit methods for integration in time.

Waveform relaxation error bounds derived in [16] show that the convergence of waveform relaxation schemes is faster if the schemes are applied to ODEs or functional ODEs systems with matrices whose entries are of smaller magnitude than if the same schemes are applied to systems with matrices whose entries are larger. For this reason we use the Kosloff and Tal-Ezer transformation which "preconditions" the Chebyshev pseudospectral matrix, making most of the entries smaller, and in addition, making the eigenvalues with large magnitude smaller. One would therefore expect, and we will show, that the convergence of waveform relaxation applied to the preconditioned matrices is faster than with the Chebyshev pseudospectral matrices which are not treated by the Kosloff and Tal-Ezer transformation.

Waveform relaxation methods for pseudospectral semi-discrete systems have been studied in [14], [3], [16] and [9]. The only work where the Kosloff and Tal-Ezer transformation was applied was in [3]. In that paper they solved the homogeneous heat equation with constant coefficients, while here we solve hyperbolic, parabolic and mixed equations, with non-constant coefficients and with functional terms. In addition, in [3], the parameter in the Kosloff and Tal-Ezer transformation was chosen as a function of N, the number of grid points in the spatial domain, while here we will show results from

3

a wider range of parameter choices. We derive the conclusion that the rate of convergence increases with increasing $\alpha \in (0, 1]$, for all types of problems mentioned above, and our conclusion is confirmed by numerical experiments. We must emphasize, however, that choosing $\alpha \approx 1$ is optimal only in the case where the spatial derivative of the solution at the boundaries is near zero. This is a reasonable assumption considering that in many applications, especially those involving diffusion, where the solution tends to zero. Consider the following physical models all of which have solutions with zero spatial derivatives specified at the boundaries [15]: A vibrating string that is free to move transversally without resistance, heat conduction where the object through which the heat is flowing is perfectly insulated, electric potential in a cylinder that is sealed to prevent the current from flowing across the boundary, or fluid velocity that is zero at the boundaries.

The organization of the paper is the following. The pseudospectral spatial discretization for (1.1) is given in Section 2. Section 3 describes the Kosloff and Tal-Ezer transformation. The waveform relaxation method for the resulting semi-discrete systems is presented in Section 4 and error bounds are introduced. Section 5 presents results from numerical experiments. We end with some concluding remarks in Section 6.

2 Pseudospectral spatial discretization for functional problem (1.1)

We apply the process of pseudospectral semi-discretization with the Chebyshev-Gauss-Lobatto points $x_i = -L \cos(\pi i/N)$, $i = 0, \ldots, N$. Let $u_i(t) = u(x_i, t)$, then the pseudospectral spatial discretization gives the following system of functional ODEs

$$
\begin{aligned}
\frac{d}{dt} u_i(t) &= \epsilon \sum_{j=1}^{N-1} d_{i,j}^{(2)} u_j(t) + c \sum_{j=\text{sign}(\epsilon)}^{N-1} d_{i,j}^{(1)} u_j(t) + g(x_i, t, (u_i)_t) \\
&\quad + \epsilon \left[d_{i,0}^{(2)} f_-(t) + d_{i,N}^{(2)} f_+(t) \right] \qquad (2.4) \\
&\quad + c \left[\text{sign}(\epsilon) d_{i,0}^{(1)} f_-(t) + d_{i,N}^{(1)} f_+(t) \right], \ 0 < t \le T, \\
u_i(t) &= f_0(x_i, t), \ -\tau_0 \le t \le T, \ i = \text{sign}(\epsilon), \ldots, N-1.
\end{aligned}
$$

Here, $D^{(1)} = [d_{i,j}^{(1)}]_{i,j=0}^N$ and $D^{(2)} = [d_{i,j}^{(2)}]_{i,j=0}^N$ are the pseudospectral differentiation matrices of the first and second order respectively, based on the grid

4

points $\{x_j\}_{j=0}^N$, cp. eg. [4], [7]. The functional argument $(u_i)_t$ for $0 < t \leq T$ is defined by

$$(u_i)_t(\tau) = u_i(t + \tau), \quad -\tau_0 \leq \tau \leq 0.$$

To have the system (2.4) written in a matrix form we introduce the notations

$$U(t) = (u_{\text{sign}(\epsilon)}(t), \ldots, u_{N-1}(t))^T \quad \widetilde{f}_0(t) = (f_0(x_{\text{sign}(\epsilon)}, t), \ldots, f_0(x_{N-1}, t))^T,$$
$$\widetilde{D}^{(2)} = [d_{i,j}^{(2)}]_{i,j=1}^{N-1}, \quad \widetilde{D}^{(1)} = [d_{i,j}^{(1)}]_{i,j=\text{sign}(\epsilon)}^{N-1}, \widetilde{d}_0^{(l)} = [d_{\text{sign}(\epsilon),0}^{(l)}, \ldots, d_{N-1,0}^{(l)}]^T \text{(2.5)}$$
$$\widetilde{d}_N^{(l)} = [d_{\text{sign}(\epsilon),N}^{(l)}, \ldots, d_{N-1,N}^{(l)}]^T, \quad l = 1, 2$$
$$\widetilde{g}(t, U_t) = (g(x_{\text{sign}(\epsilon)}, t, (u_{\text{sign}(\epsilon)})_t), \ldots, g(x_{N-1}, t, (u_{N-1})_t))^T.$$

Now the problem (2.4) can be written in the following form

$$\begin{aligned}
\frac{d}{dt} U(t) &= \left[\epsilon \widetilde{D}^{(2)} + c \widetilde{D}^{(1)}\right] U(t) + \widetilde{g}(t, U_t) + \epsilon \left[f_-(t) \widetilde{d}_0^{(2)} + f_+(t) \widetilde{d}_N^{(2)}\right] \\
&\quad + c \left[\text{sign}(\epsilon) f_-(t) \widetilde{d}_0^{(1)} + f_+(t) \widetilde{d}_N^{(1)}\right], \quad 0 < t \leq T, \qquad (2.6) \\
U(t) &= \widetilde{f}_0(t), \quad -\tau_0 \leq t \leq 0.
\end{aligned}$$

In the next section we describe the Kosloff and Tal-Ezer transformation applied to (2.6).

3 Grid transformation for the functional problem (2.6)

We consider the Kosloff and Tal Ezer grid transformation $y = g_\alpha(x)$ where the Chebyshev grid $x_i = -L \cos(\pi i/M)$ is stretched by the parameter dependent, continuous transformation $g_\alpha : [-L, L] \to [-L, L]$:

$$y = g_\alpha(x) = \frac{\sin^{-1}(\alpha x)}{\sin^{-1}(\alpha)}, \quad 0 < \alpha \leq 1. \qquad (3.7)$$

As $\alpha \to 0$ the grid approaches the Chebyshev grid, while as $\alpha \to 1$ the grid approaches an equally spaced grid.

In order to solve a given partial differential equation in variable $u(y, t)$, on the transformed grid, the grid values $u(y_j, t)$ must be used to obtain values for the spatial derivatives of u of any order. This is accomplished via repeated application of the chain rule to re-express spatial derivatives of

5

$u(y,t)$ in terms of spatial derivatives of $u(x,t)$ with respect to x, yielding, for example, for the first order derivative

$$\frac{du}{dy}(y_i, t) \cong \frac{1}{g'_\alpha(x_i)} \sum_{j=0}^{N} d_{ij}^{(1)} u(y_j, t), \qquad (3.8)$$

[10]. Here the entries $d_{ij}^{(1)}$ are still the entries of the matrix $D^{(1)}$, which approximate the first order differential operator on the Chebyshev grid. On the stretched grid, the operator $D^{(1)}$ is replaced by $D_\alpha^{(1)} = A^{(1)} D^{(1)}$, where $A^{(1)}$ is a diagonal matrix with entries

$$A_{kk}^{(1)} = \frac{1}{g'_\alpha(x_k)} = \frac{\sin^{-1}(\alpha)\sqrt{1 - \alpha^2 x_k^2}}{\alpha}.$$

Note that $A_{kk}^{(1)}$ increases from $O(1/N)$ at $k = 0$, to $O(1)$ for k at the middle of the matrix, and then decreases back to $O(1/N)$ for $k = N$.

The operators for higher order derivatives are obtained in a similar fashion, [10, 13]. Here we will need the second order derivative operator

$$\frac{d^2}{dy^2} \approx (A^{(1)})^2 D^{(2)} - A^{(2)} D^{(1)} \qquad (3.9)$$

$$\equiv D_\alpha^{(2)}$$

where $D^{(2)}$ is the second order operator for the original grid, and $A^{(2)}$ is the diagonal matrix with entries

$$A_{kk}^{(2)} = g''_\alpha(x_k)/(g'_\alpha(x_k))^3 = \left(\sin^{-1}(\alpha)\right)^2 x_k.$$

We note that this operator (3.9) is not equivalent to $(A^{(1)} D^{(1)})^2$.

The more severe scaling with α tending to 1 permits the use of larger time steps in explicit schemes, however, in the limit, at $\alpha = 1$, we are left with a high order interpolant on an equally spaced grid. It is well known that this causes Runge phenomenon, and if one were to input a near equally spaced grid into Fornberg's algorithm [7] to calculate the derivative (3.8) or (3.9) the approximation would be unstable.

Alternatively, we view the transformation as preconditioning the Chebyshev pseudospectral derivative matrices with matrices $A^{(1)}$, for example, in

6

the first derivative calculation. The only potential problem with this viewpoint is that when $\alpha = 1$, the matrix $A^{(1)}$ has entries $A_{00} = A_{NN} = 0$, and the homogeneous Neumann boundary conditions

$$\frac{\partial}{\partial x}u(-1,t) = \frac{\partial}{\partial x}u(1,t) = 0,$$

are imposed on the solution u. In this work this is not a problem because the spatial derivative of the solution is nearly zero at the endpoints. We will show that in this case, choosing $\alpha = 1$ is optimal for both convergence and accuracy.

The Kosloff and Tal-Ezer transformation gives new matrices and vectors

$$\widetilde{D}^{(2)}_\alpha, \widetilde{D}^{(1)}_\alpha, \tilde{d}^{(2)}_{0,\alpha}, \tilde{d}^{(2)}_{N,\alpha}, \tilde{d}^{(1)}_{0,\alpha}, \tilde{d}^{(1)}_{N,\alpha}, \tag{3.10}$$

which we use for (2.6). Note here that we use the convention that $\alpha = 0$ gives the matrix form at the Chebyshev points.

4 Waveform relaxation for (2.6)

We simplify the system (2.6) by splitting each of the matrices $\widetilde{D}^{(l)}_\alpha$, $l = 1, 2$ into two matrices:
$$\widetilde{D}^{(l)}_\alpha = A^{(l)}_\alpha + B^{(l)}_\alpha, \quad l = 1, 2. \tag{4.11}$$

In this section we consider waveform relaxation schemes based on the general splitting (4.11) and derive an error bound for such general schemes. In the next section we will study Jacobi waveform relaxation schemes based on the following special splitting

$$A^{(l)}_\alpha = diag(\widetilde{D}^{(l)}_\alpha), \quad B^{(l)}_\alpha = \widetilde{D}^{(l)}_\alpha - diag(\widetilde{D}^{(l)}_\alpha). \tag{4.12}$$

Since the matrices $A^{(l)}_\alpha$ are diagonal, the resulting systems of differential equations can be integrated in a parallel computing environment. Let

$$\begin{aligned} \tilde{A}_\alpha &= \epsilon A^{(2)}_\alpha + c A^{(1)}_\alpha \\ \tilde{B}_\alpha &= \epsilon B^{(2)}_\alpha + c B^{(1)}_\alpha. \end{aligned} \tag{4.13}$$

Then solutions $U(t)$ to the system (2.6) can be approximated by successive iterates $U^k(t)$ computed according to the following waveform relaxation

7

scheme

$$
\begin{aligned}
\frac{d}{dt}U^{k+1}(t) \;=\;& \tilde{A}_\alpha U^{k+1}(t)+\tilde{B}_\alpha U^k(t)+\tilde{g}(t,U^k_t) \\
&+\epsilon\left[f_-(t)\tilde{d}^{(2)}_{0,\alpha}+f_+(t)\tilde{d}^{(2)}_{N,\alpha}\right] \\
&+c\left[\mathrm{sign}(\epsilon)f_-(t)\tilde{d}^{(1)}_{0,\alpha}+f_+(t)\tilde{d}^{(1)}_{N,\alpha}\right],\quad 0<t\le T, \\
U^{k+1}(t) \;=\;& \tilde{f}_0(t),\quad -\tau_0\le t\le 0.
\end{aligned}
\tag{4.14}
$$

Here, $k=0,1,\ldots$, and $U^0(t)$ is an arbitrary starting function. If the matrix $A^{(l)}_\alpha$ is diagonal (Jacobi waveform relaxation), then each equation of the system (4.14) can be solved independently by a different processor.

In this paper we study how the convergence of the iteration scheme (4.14) depends on the parameter α. Therefore, we shall study the error

$$
e^k(t)=U^k(t)-U(t).
$$

Let $\|\cdot\|$ be an arbitrary vector norm or the induced matrix norm. For an arbitrary matrix M we define

$$
\mu(M)=\lim_{\epsilon\to 0^+}\frac{\|I+\epsilon M\|-1}{\epsilon}
$$

the logarithmic norm of the matrix M, where I is an identity matrix. To derive an error bound for $e^k(t)$ we need the following.

Assumption 4.1 *Suppose that there exists a positive constant ν such that*

$$
\|\tilde{g}(t,U)-\tilde{g}(t,\overline{U}_t)\|\le \nu\max\{\|U(\tau)-\overline{U}(\tau)\|:t-\tau_0\le\tau\le t\}
\tag{4.15}
$$

for $t\in[0,T]$, $U,\overline{U}\in C([-\tau_0,T],R^{N-\mathrm{sign}(\epsilon)})$, and $\tilde{g}(t,\overline{U}_t)$ defined in (1.2) or (1.3).

The error bound for $e^k(t)$ is given in the following theorem.

Theorem 4.2 *Suppose that Assumption 4.1 is satisfied. Then*

$$
\|e^{k+1}(t)\|\le \frac{(\|\tilde{B}_\alpha\|+\nu)^{k+1}}{k!}\int_0^t s^k e^{s\mu(\tilde{A}_\alpha)}ds\max_{0\le\tau\le t}\|e^0(\tau)\|,
\tag{4.16}
$$

for $t\in[0,T]$.

8

Proof: Subtracting (2.6) (with the matrices and vectors specified in (3.10)) from (4.14) gives

$$\frac{d}{dt}e^{k+1}(t) - [\epsilon A_\alpha^{(2)} + cA_\alpha^{(1)}]e^{k+1}(t) = [\epsilon B_\alpha^{(2)} + cB_\alpha^{(1)}]e^k(t) + \tilde{g}(t, U_t^k) - \tilde{g}(t, U_t). \tag{4.17}$$

Using the notation (4.13), multiplying (4.17) by $e^{-\tilde{A}_\alpha t}$ from the left-hand side, integrating from 0 to t and then multiplying the resulting equation by $e^{\tilde{A}_\alpha t}$ again from the left-hand side gives

$$e^{k+1}(t) = \int_0^t e^{\tilde{A}_\alpha(t-s)} \left(\tilde{B}_\alpha e^k(s) + \tilde{g}(s, U_s^k) - \tilde{g}(s, U_s) \right) ds. \tag{4.18}$$

From (4.18) and Assumption 4.1 we have

$$\|e^{k+1}(t)\| \le \left(\|\tilde{B}_\alpha\| + \nu \right) \int_0^t e^{\mu(\tilde{A}_\alpha)(t-s)} \max_{0 \le \tau \le s} \|e^k(\tau)\| ds. \tag{4.19}$$

From (4.19) we have (4.16) for $k = 0$. We now suppose (4.16) for $k - 1$ and using (4.19) prove (4.16) for k. From (4.19) and from (4.16) with $k + 1$ replaced by k we have

$$\|e^{k+1}(t)\| \le \frac{(\|\tilde{B}_\alpha\| + \nu)^{k+1}}{(k-1)!} \int_0^t e^{\mu(\tilde{A}_\alpha)(t-z)} \int_0^z s^{k-1} e^{\mu(\tilde{A}_\alpha)s} ds dz \max_{0 \le \tau \le t} \|e^0(\tau)\|. \tag{4.20}$$

Since

$$\int_0^t e^{\mu(\tilde{A}_\alpha)(t-z)} \int_0^z s^{k-1} e^{\mu(\tilde{A}_\alpha)s} ds dz = \frac{1}{k} \int_0^t s^k e^{\mu(\tilde{A}_\alpha)s} ds,$$

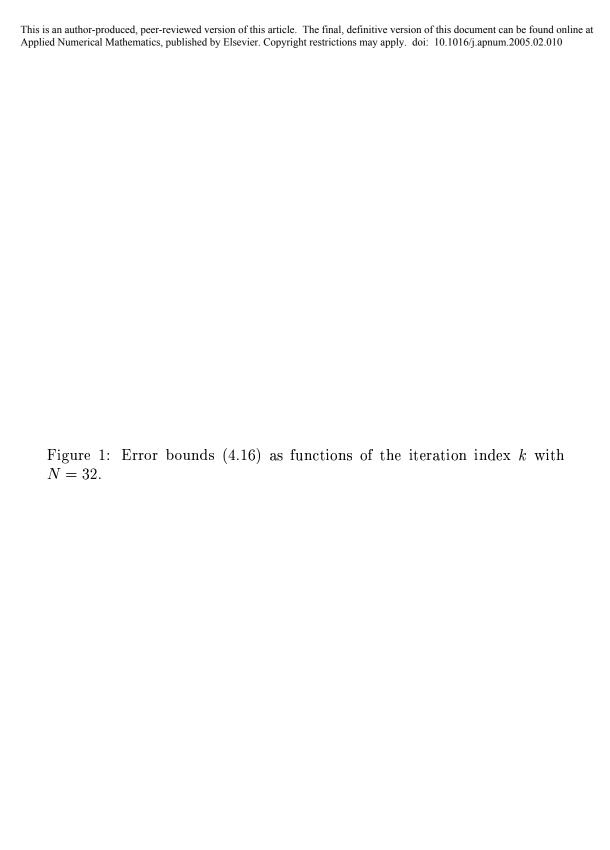(4.16) follows from (4.20), which finishes the proof. □

We study the error bound (4.16) with $\tilde{A}_\alpha$ and $\tilde{B}_\alpha$ defined by (4.13) as a function of the waveform relaxation iteration index k in Figure 1, and as a function of the parameter α in the Kosloff and Tal-Ezer transformation in Figure 2, when $N = 32$. The problem in both Figures is posed on $[-10, 10] \times [0, 1]$ and the error bounds are computed at $t = 1$. Results from the problem without delay are not shown because even though the error bounds are smaller, the results are similar to results from the delay case shown here. For the delay term we choose the value $\nu = 5$ for the functions g from the family which satisfies the Lipschitz condition, Assumption 4.1.

In Figure 1 the error bounds from the hyperbolic problem ($\epsilon = 0$, $c = 1$), the parabolic problem ($\epsilon = 1$, $c = 0$), and the mixed problem ($\epsilon = c = 1$) are

9

shown. In each of the graphs α is held fixed, and the three lines represent $\alpha = 0, 0.9, 1$. We see significant improvement in convergence of waveform relaxation when $\alpha = 0.9$ and $\alpha = 1$. Convergence is obtained with $\alpha = 0$, however it takes more iterations, i.e. $k > 300$ for the Chebyshev case. We also note that the diffusive part of the mixed hyperbolic-parabolic problem dominates the error bound.

In Figure 2 we plot the error bound as a function of $\alpha \in [0, 1]$ for three different iteration indices: $k = 100, 120, 140$. We show results from only the hyperbolic and parabolic problems because, as in Figure 1, the results from the mixed problem are similar to the results from the parabolic problem. In the parabolic problem it appears as though the error is increasing for increasing iteration index k when $\alpha < 0.7$. This is because for these values of α, and when $100 \leq k \leq 140$, there is a "hump" in the error bound, as seen in Figure 1. On the other hand, when $\alpha > 0.7$, the error as a function of k is strictly decreasing at $k = 100$. In the hyperbolic problem the error as a function of k is strictly decreasing at $k = 100$ for all values of α, thus the curves are uniform. More importantly, we conclude from Figure 2 that for all cases (hyperbolic, parabolic, mixed, no delay, and with delay), and for fixed k, the error bounds are decreasing as α increases with the fastest convergence of waveform relaxation at $\alpha = 1$.
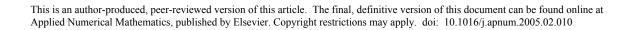
10

Figure 1: Error bounds (4.16) as functions of the iteration index k with $N = 32$.

11

Figure 2: Error bounds (4.16) as functions of α with $N = 32$.

In the next section we present the errors $\|e^k(t)\|$ for extensive numerical data obtained by applying (4.14) with the Jacobi splitting (4.12) for the matrices $\widetilde{D}_\alpha^{(2)}, \widetilde{D}_\alpha^{(1)}$ with $\alpha \in [0, 1]$. It will be shown that the errors $\|e^k(t)\|$ behave like their error bounds (i.e. they decrease as α increases).

5 Numerical experiments

In this section we present results of numerical experiments for the following test problem

$$\frac{\partial u}{\partial t}(x,t) = \epsilon\frac{\partial^2 u}{\partial x^2}(x,t) + c\frac{\partial u}{\partial x}(x,t) - \nu u(x,t-\tau_0) + g(x,t), \quad -L \leq x \leq L, \ 0 < t \leq T,$$
$$u(\pm L, t) = f_\pm(t), \quad 0 < t \leq T, \tag{5.21}$$
$$u(x,t) = f_0(x,t), \quad -\tau_0 \leq t \leq 0, \ -L \leq x \leq L.$$

We select the right-hand side function $g(x,t)$, and the initial and boundary functions $f_0(x,t)$ and $f_\pm(t)$, in such a way that the solution of the problem is known exactly and equal to $u(x,t) = t\exp(-x^2)$. We choose $L = 10$, thus the boundary functions are $f_\pm(t) = t\exp(-L^2)$ (nearly zero), and we integrate until $T = 1$. As in Section 4 we consider six problems: the advective-diffusive problem ($\epsilon = c = 1$), the diffusive problem ($\epsilon = 1, c = 0$) and the hyperbolic problem ($\epsilon = 0, c = 1$) each with $\nu = 0$ and $\tau_0 = 0$ (non-delay case) and with $\nu = 5$ and $\tau_0 = 0.1$ (delay case).

The waveform relaxation scheme (4.14) for the problem (5.21) is written in the following form

$$\frac{d}{dt}U^{k+1}(t) = \widetilde{A}_\alpha U^{k+1}(t) + \widetilde{B}_\alpha U^k(t) - \nu U^k(t - \tau_0) + \overline{g}(t) + f(t), \quad 0 < t \leq T,$$
$$U^{k+1}(t) = \widetilde{f}_0(t), \quad -\tau_0 \leq t \leq 0. \tag{5.22}$$

Here,

$$\overline{g}(t) = (g(x_{sign(\epsilon)}, t), \ldots, g(x_{N-1}, t))^T,$$
$$f(t) = \epsilon\left[f_-(t)\widetilde{d}_{0,\alpha}^{(2)} + f_+(t)\widetilde{d}_{N,\alpha}^{(2)}\right] + c\left[sign(\epsilon)f_-(t)\widetilde{d}_{0,\alpha}^{(1)} + f_+(t)\widetilde{d}_{N,\alpha}^{(1)}\right].$$

The initial function $\widetilde{f}_0$ is defined in (2.5). If the matrices $\widetilde{A}_\alpha$ and $\widetilde{B}_\alpha$ are defined by (4.13), then (5.22) is Jacobi waveform relaxation scheme which we use for our numerical experiments.

13

To integrate the systems (5.22) in time we use the BDF3 method with the time step $n\Delta t = 1.0$. Integration of the systems (5.22) results in the approximations $U_{i,n}^k \approx U_i(n\Delta t)$, $n = 1, 2, \ldots$. We study the errors

$$e_\alpha^k(n\Delta t) = \max_{i=0,\ldots,N-1} |U_{i,n}^k - u(x_i, n\Delta t)| \qquad (5.23)$$

measured at $n\Delta t = 1$ which can be compared with their upper bounds (4.16) plotted in Figures 1 and 2.

In Figure 3 we present the errors (5.23) as functions of the iteration index k, when $N = 32$ and for $\alpha = 0$, $\alpha = 0.9$, and $\alpha = 1$. The upper bound for this error curve is shown in Figure 1, and the actual errors are expectedly much smaller than their bounds. However, similar to the bounds, we do see that the error curve corresponding to $\alpha = 0$ has a larger "hump" (compared to $\alpha = 0.9, 1$), and that it decays more slowly. Since the errors (5.23) include not only the waveform relaxation error, but also the spatial and time discretization errors, the curves in Figure 3 become horizontal lines after a given number of iterations, which we define by k_{max}. The fact that the error curves become horizontal after k_{max} indicates that the waveform relaxation errors are smaller than the spatial and time discretization errors, thus the horizontal lines represent the spatial and time discretization errors.

As predicted in Figure 1 the number k_{max} in each picture of Figure 3 is the largest for $\alpha = 0$, smaller for $\alpha = 0.9$ and the smallest for $\alpha = 1$. We denote these numbers by $k_{max}(0)$, $k_{max}(0.9)$, $k_{max}(1)$, respectively. The number $k_{max}(1)$ is about three times smaller than $k_{max}(0)$ in case of parabolic and mixed problems. For hyperbolic problem the number $k_{max}(1)$ is about four times smaller than $k_{max}(0)$.

In Figure 4 we plot the errors (5.23) as functions of α, two of which can be compared with the error bounds plotted in Figure 2. Errors from the problem without a delay term are also plotted in Figure 4 since we see different behavior than with the delay term. The three lines in each of the six cases represent the errors at three iteration indices $k_{max}(0)$, $k_{max}(0.9)$, $k_{max}(1)$. Note that each of these iteration indices are different for each of the six problems.
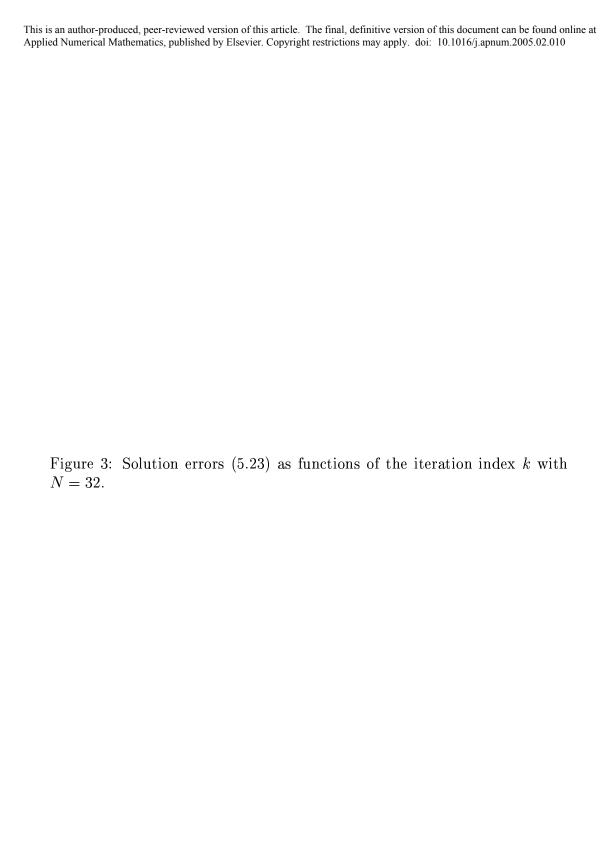
In Figure 4 it again appears (as in Figure 2) that for many of the problems, larger error occurs with larger iteration index, for certain values of α. This again is due to the "hump" in the error before it decreases as a function of k. The fact that the solid line is nearly horizontal in all graphs in Figure 4 indicates that by $k_{max}(0)$, i.e. by the time waveform relaxation with the

14

Chebyshev pseudospectral method converges, most choices of $\alpha < 1$ have previously converged. The solid line decreasing near $\alpha = 1$ indicates that the accuracy of the solution is better with these choices of α.

In each of the graphs in Figure 4 the dotted and dot-dashed lines (which were plotted for $k_{max}(0.9)$, $k_{max}(1)$, respectively) join the solid lines (plotted for $k_{max}(0)$) at certain points α^* (each line has a different point α^*). For $\alpha \geq \alpha^*$ the corresponding lines are covered by the solid lines. The dotted lines for $\alpha < \alpha^*$ (with α^* which correspond to them) show that the numbers $k_{max}(0.9)$ are too small for the iteration process to make the waveform relaxation errors smaller than the spatial and time discretization errors. In other words, for these choices of $\alpha < \alpha^*$ and $k < k_{max}(0.9)$ the errors (5.23) as functions of k are still during their humps before reaching their constant levels. Similar phenomena happen for dot-dashed lines. Our concluding remarks for Figure 4 are that for increasing α, we see decreasing error at fixed iteration index k, with the best accuracy at $\alpha = 1$.

It is widely believed that α should be chosen as a function of N, so in Figure 5 we hold α fixed and show errors with different values of N. Results in 5 are with the extreme values of parameter choices: $\alpha = 0$ (on the left) and $\alpha = 1$ (on the right). Results from the non-delay case are omitted because they are similar to the delay case, while results from the mixed problem are omitted because they are similar to the parabolic problem.

Our conclusions do not change, given the results in Figure 5. What we do see there is that in all cases it takes longer for waveform relaxation to converge as N increases, but when it does converge, the error is smaller with larger N. This is because the larger the value of N, the more ill-conditioned the derivative matrices. In addition, since the transformation smooths the Chebyshev differentiation matrix, the accuracy of the solution with $\alpha = 1$ is significantly better in the beginning iterations. Not only does the choice $\alpha = 1$ converge more quickly, the overall error is also orders of magnitude smaller.
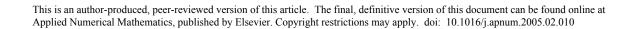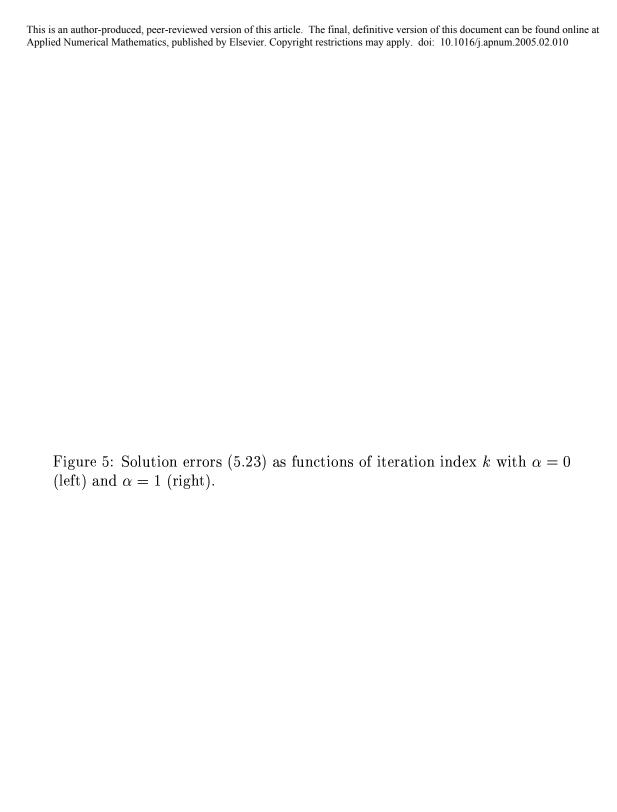
15

Figure 3: Solution errors (5.23) as functions of the iteration index k with $N = 32$.

Figure 4: Solution errors (5.23) as functions of α with $N = 32$.

17

Figure 5: Solution errors (5.23) as functions of iteration index k with $\alpha = 0$ (left) and $\alpha = 1$ (right).

18

6 Concluding remarks

The Chebyshev pseudospectral spatial discretization with the Kosloff and Tal-Ezer transformation [10] was applied to hyperbolic, parabolic, and mixed hyperbolic-parabolic differential-functional problems. The resulting semi-discrete system was solved by the Jacobi waveform relaxation method, thus the equations of the system were separated in such a way that each of them can be solved by a different processor in parallel. We studied the relationship between the convergence of the Jacobi waveform relaxation scheme and the parameter α in the transformation. In addition, we derived a new error bound for the waveform relaxation method, which says that waveform relaxation converges more quickly as α increases from 0 to 1. Numerical results from hyperbolic, parabolic, and mixed hyperbolic-parabolic functional equations with and without delay terms confirm that as α increases, waveform relaxation converges faster. Numerical results also show that the errors in the solution decrease as α increases with the best accuracy and fastest converge occurring at $\alpha = 1$ when the solution has zero spatial derivatives at the boundaries.

The Kosloff and Tal-Ezer transformation is typically used to allow larger time steps in explicit schemes for the solution of partial differential equations. Choosing $\alpha = 1$ allows the largest time step, but it also amounts to approximating the derivative with high order interpolant on an equally spaced grid, so traditionally $\alpha = 1$ is not chosen. However, if we view this transformation as preconditioning the Chebyshev pseudospectral differentiation matrices, and the solution has zero derivative values at the boundaries, choosing $\alpha = 1$ not only results in the fastest convergence of waveform relaxation, but also results in the most accurate solution with waveform relaxation.

It was previously shown that the waveform relaxation error bounds and convergence are better with the Chebyshev pseudospectral method than with finite differences [16]. In [3] it was shown for the heat equation that the Kosloff and Tal-Ezer transformation can improve the convergence of waveform relaxation when α is chosen as a function of N. Here, for hyperbolic, parabolic and mixed functional equations we derive error bounds for waveform relaxation with the Kosloff and Tal-Ezer transformation and determine that choosing $\alpha = 1$ is optimal when the solution has zero spatial derivatives at the boundaries.

19

References

[1] B. Basse, B. C. Baguley, E. S. Marshall, W. R. Joseph, B. van Brunt, G. Wake, D. J. N. Wall, A mathematical model for analysis of the cell cycle in human tumors, to appear in *J. Mathematical Biology*.

[2] K. Burrage, Parallel and Sequential Methods for Ordinary differential equations, Oxford University Press, Oxford 1995.

[3] K. Burrage, Z. Jackiewicz, R. A. Renaut, The performance of preconditioned waveform relaxation techniques for pseudospectral methods, *Numer. Methods Partial Differential Equations* **12** (1996) 245-263.

[4] C. Canuto, M. Y. Hussaini, A. Quarteroni, T. A. Zang, Spectral Methods in Fluid Dynamics, Springer-Verlag, 1988.

[5] C. J. Chyan, G. F. Webb, A model of proliferating cell populations with correlation of mother-daughter mitotic times, Ann. Mat. Pura Appl. 157 (1991), 1-11.

[6] W.S. Don and A. Solomonoff, Accuracy enhancement for higher derivatives using Chebyshev collocation and a mapping technique, *SIAM J. Sci. Comput.* Vol. 18, No. 4, pp. 1040-1055, July 1997.

[7] B. Fornberg, A Practical Guide to Pseudospectral Methods, Cambridge University Press, 1996.

[8] J.S. Hesthaven, P. G. Dinesen, and J.P. Lynov, Spectral collocation time-domain modelling of diffractive optical elements, *J. Comput. Phys.* 155, pp. 287-306, 1999.

[9] Z. Jackiewicz, B.D. Welfert, B. Zubik-Kowal, Spectral versus pseudospectral solutions of the wave equation by waveform relaxation methods, to appear in *J. Sci. Comput.*

[10] D. Kosloff and J. Tal-Ezer, A modified Chebyshev pseudospectral method with an $O(N^{-1})$ time step restriction, *J. Comput. Phys.* 104, pp. 457-469, 1993.

[11] J. Mead and R. Renaut, Accuracy, Resolution, and Stability Properties of a Modified Chebyshev Method, *SIAM J. Sci. Comput* 24, No. 1, pp. 148-160, 2002.

[12] R. Renaut and J. Frohlich, A Pseudospectral Chebychev Method for the 2D Wave Equation with Domain Stretching and Absorbing Boundary Conditions, *J. Comput. Phys.* 124, pp. 324-336, 1996.

[13] R. Renaut and Y. Su, Evaluation of Chebychev Pseudospectral Methods for Third Order Differential Equations, *Numerical Algorithms* 16, pp. 255-281, 1997.

[14] R. E. Spilling, Dynamic iteration and the pseudospectral method, *Student Report*, Department of Mathematical Sciences, The Norwegian Institute of Technology, Trondheim, Norway, 1993.

[15] W. A. Strauss, "Partial Differential Equations An Introduction", John Wiley & Sons, Inc, New York, 1992.

[16] B. Zubik-Kowal, Chebyshev pseudospectral method and waveform relaxation for differential and differential-functional parabolic equations, *Appl. Numer. Math.* **34** (2000), 309-328.

21